Multistate curve-crossing model for scattering: Associative ionization and excitation transfer in helium*

James S. Cohen

Theoretical Division (T-6), Los Alamos Scientific Laboratory, University of California, Los Alamos, New Mexico 87544

(Received 2 June 1975)

A model has been derived to treat the multistate curve-crossing problem which often arises in diabatic representations of scattering processes. Transitions between diabatic states are assumed to occur only in the vicinity of curve crossings and the probabilities are evaluated semiclassically. Otherwise the nuclear trajectories are treated classically except for tunneling through long-range potential barriers taken into account by the JWKB approximation. Closed channels are included on an equal footing with the scattering channels. The model is applied to the problems of symmetric associative (and dissociative) ionization and excitation transfer in collisions of excited helium with the ground-state atom, using the diabatic representation for the Rydberg states of He_2 presented in the preceding paper. The electronic coupling of the repulsive diabatic states in the continuum yields much larger ionization cross sections than does direct vibronic coupling of low-lying adiabatic states to the continuum. The diabatic-states model is shown to be a valid interpretation of associative ionization in helium. Ionization has a significant effect on some excitation-transfer cross sections. Integrated cross sections are presented for ionization of helium in the $n\,^3S$, $n\,^3P$, and $n\,^3D$ states, $n = 3,4$, and for excitation transfer from the $n = 3$ states to states with $2 \leq n \leq 4$ for collision energies from thermal to 100 eV. The thermally averaged associative ionization cross sections, in units of 10^{-16} cm^2, obtained at 300°K are as follows: $\bar{Q}_i(3\,^3S) = 0.06$, $\bar{Q}_i(3\,^3P) = 2.0$, $\bar{Q}_i(3\,^3D) = 2.9$, $\bar{Q}_i(4\,^3S) = 0.6$, $\bar{Q}_i(4\,^3P) = 1.7$, and $\bar{Q}_i(4\,^3D) = 4.3$. The results are in quite satisfactory agreement with recent experiments.

I. INTRODUCTION

Helium discharges and afterglows have been studied experimentally for many years, but the experiments are complex and knowledge of cross sections for collisional ionization, recombination, and energy transfer is still very limited. To determine the effects of different experimental conditions it is very helpful to know what the important excitation and relaxation mechanisms are and to find the energy dependences of the corresponding cross sections. The present work was undertaken to examine a postulated theoretical mechanism for associative ionization (AI, often referred to as the Hornbeck-Molnar process),

$$\mathrm{He}^*(n^{2s+1}L) + \mathrm{He}(1\,^1S) \rightarrow \mathrm{He}_2^+(v) + e\,, \tag{1}$$

and to obtain cross sections for this reaction and the excitation-transfer (ET) process,

$$\mathrm{He}^*(n^{2s+1}L) + \mathrm{He}(1\,^1S) \rightarrow \mathrm{He}^*(n'^{\,2s+1}L') + \mathrm{He}(1\,^1S)\,. \tag{2}$$

After Tüxen[1] first identified He_2^+, Arnot and M'Ewen[2] demonstrated that one source of the molecular ion was the two-body reaction (1) and suggested that He* could be, among other states, the $2\,^3S$ metastable state of helium at 19.8 eV. Later, Meyerott[3] deduced from collision-enhanced spectra that 22.5 ± 0.5 eV was required to form He_2^+ in its ground vibrational state from two helium atoms, and Hornbeck[4] observed that the molecular ions were formed less than 10^{-6} sec after the initial electron excitation. Motivated by these findings, Hornbeck and Molnar[5] reinvestigated the appearance potential of He_2^+ and found it to be between 22.5 and 23.4 eV. Hence excitation of He* to $n \geq 3$ was established as a necessary, though not sufficient, condition for associative ionization in helium to occur. More recent measurements, establishing the appearance potential at about 23.1 eV, appear to rule out participation of the $3\,^3S$ and $3\,^1S$ states.[6-9] This value may be compared[10] to the value 22.22 eV, given by $E_i(\mathrm{He}) - D_e(\mathrm{He}_2^+) + E_{v=0}(\mathrm{He}_2^+) = 24.58 - 2.47 + 0.11$ eV,[11,12] which is the minimum energy required to form He_2^+ in its ground state and which would allow participation by the $3\,^{1,3}S$ states though still not by states with $n < 3$. The higher actual appearance potential has been interpreted as implying that the He_2^+ resulting from associative ionization is vibrationally excited, a conclusion consistent with the observation that the inverse process, dissociative recombination, apparently does not occur for unexcited[13] He_2^+.

Mulliken[13] proposed a qualitative model for associative ionization in helium involving crossings of B-core Rydberg states of He_2, which result from addition of an electron to the repulsive $B(\sigma_g\sigma_u^2, {}^2\Sigma_g^+)$ state of He_2^+, into the continuum delimited by the potential curve for the attractive $A(\sigma_g^2\sigma_u, {}^2\Sigma_u^+)$ ground state of He_2^+. He suggested that these B-core states dissociate to $\mathrm{He} + \mathrm{He}^+ + e$ and have deep stable minima at distances larger than the He_2^+ equilibrium distance. The higher-lying A-core

states would cross such partially diabatic B-core states twice, and if a transition between these states occurred at the inner crossing but not at the outer crossing (or vice versa), associative ionization could result.

We find it somewhat more convenient for a mathematical description of the scattering to use fully diabatic orthogonal states. With such a representation, given in the preceding paper (hereafter referred to as I),[12] the B-core curves cross into the continuum in a manner similar to Mulliken's hypothetical potential curves, but are entirely repulsive (except possibly for the Van der Waals region) and dissociate to He + He* in low-lying excited states.[14]

Gillen *et al.*,[15] using the calculated transition probabilities of Evans *et al.*[16] for the lowest $^3\Sigma_g^+$ diabatic states and neglecting higher Rydberg states, have shown that such a diabatic mechanism is responsible for collisional ionization in He($2\,^3S$) + He($1\,^1S$) collisions. The mechanism for excitation transfer from states with $n \geq 3$ is also transparent in this representation. The model derived to treat the multistate curve-crossing problem considers the various crossings to be independent and neglects interference effects. This treatment has similarities to the trajectory surface hopping approach of Tully and Preston to reactive scattering.[17] Closed channels are included and tunneling through long-range potential barriers is accounted for in the JWKB approximation. The model satisfies the principle of detailed balancing and conserves flux, displaying cusp effects at the thresholds of opening channels.

The diabatic representation allowing curve crossings into the continuum is particularly appropriate for describing associative ionization. Koike and Nakamura[18] have distinguished two regions for associative ionization in slow collisions $A^* + B \rightarrow AB^+ + e$ depending on whether the energy of $(AB)^*$ is higher or lower than the energy of $(AB)^+$. In the case of symmetric associative ionization the ionization potential is larger than the excitation energy in the separated-atom (SA) limit (otherwise atomic autoionization could occur), and for the molecular excited-state energy to become higher than the ionized-state energy a curve crossing must occur. When the excited-state curve is the lower, only nonadiabatic coupling to the continuum can result in ionization. However, if a crossing occurs and the excited-state curve becomes the higher, the discrete and continuum states are then coupled electronically, and the effect of nonadiabaticity is expected to be negligible in comparison. Nielsen and Berry[19] have carried out calculations on associative ionization in H*($n = 3$) + H collisions by taking the nonadiabaticity term as a perturbation. There have been no measurements of associative ionization of hydrogen atoms, but their cross sections are two or three orders of magnitude smaller than the experimental results in helium. Koike and Nakamura,[18] with a different formalism but taking essentially the same coupling operator, obtained results similar to those of Nielsen and Berry. In both of these calculations the excited-state curves used were attractive and had no crossings with the ion curve. Some of the potential curves of Nielsen and Berry were diabatic with respect to other states arising from the $n = 3$ atomic manifold, but all were adiabatic with respect to the higher-lying Rydberg states, and dynamic coupling to them was neglected. No calculations have been carried out on the hydrogen system with the present model; thus it is not possible at this time to say whether or not the repulsive diabatic states of H_2, arising analogously to those of He_2 because of the similar core structure,[13] would yield larger cross sections. However, as pointed out in Paper I, coupling between many *adiabatic* Rydberg states of helium is essential to obtain the large observed cross sections. It should be recognized that for dissociative recombination of electrons with He_2^+ in the lowest vibrational states, only the nonadiabatic coupling mechanism is available and the observed cross sections are correspondingly quite small. It is important to keep in mind that associative ionization and its inverse process, dissociative recombination, are generally observed in different regions of phase space.

There have been a number of experimental studies of associative ionization[20-25] and excitation transfer[26-35] in helium since the early demonstrations already referred to. Most experiments measuring the collisional relaxation rates of excited states in helium have been based on the pressure dependence of the observed radiative lifetimes. Such indirect measurements do not distinguish between excited-state destruction by excitation transfer and associative ionization, and further assumptions must be made to separate individual cross sections. Only recently have direct measurements of these cross sections been possible.[23,24] The present work provides the first theoretical comparison to experiment, as well as energy dependencies and cross sections for other states which have not been observed. The comparison to experiment is generally good and confirms the diabatic mechanism for associative ionization in helium. The calculations show that the associative-ionization channel often has a significant effect on excitation transfer; thus a two-state approximation to calculate an excitation-transfer cross section will generally not be adequate.

A brief outline of the paper is as follows: The formalism for dealing with the general multistate curve-crossing problem is presented in Sec. II. The essential assumptions made are the following: The curve crossings are isolated; transitions occur only at the crossings and with probabilities dependent only on the potentials in the vicinity of each crossing; interference effects can be neglected; barrier penetration can be treated by the JWKB approximation; ionization occurs only via electronic coupling in the continuum and can be treated by the JWKB approximation with a local complex potential; and no nonionizing transitions occur between resonant states embedded in the electronic continuum. A simple semiclassical (Landau-Zener) description of individual curve crossings is discussed in Sec. II A, but the subsequent formulas are not dependent on this particular form. In Sec. II B, matrices describing the effects of individual attractive curves of the Rydberg series are given, with separate treatments for the cases of an open channel, a closed channel, and a channel in the continuum. Recursion relations are presented for absorbing the closed channels into an effective potential. In Sec. II C initial-condition matrices are defined and reaction probabilities for inelastic scattering and ionization are obtained in terms of the matrices derived in Sec. II B. In Sec. III formulas for the corresponding cross sections are given. It is shown that the observable cross sections are averages of cross sections for scattering with various angular-momentum components weighted by their degeneracies. In Sec. IV, the theory is applied to excitation transfer and chemi-ionization in the scattering of excited helium atoms by the ground-state helium atom. The results are compared with experiment and found to be in reasonably good agreement. Limitations of the model, imposed by the basic assumptions, and their effects on He* + He scattering calculations are discussed in Sec. V.

II. THEORY

A. Curve-crossing parameters

The scattering problem is formulated in the diabatic representation, using the potential curves and coupling matrix elements presented in Paper I for the application to He* + He collisions.[12] The diabatic Rydberg states are of two basic types, the attractive A-core states and the repulsive B-core states whose potential curves cross all the asymptotically higher A-core curves. It is assumed that all transitions between states of He_2 occur at curve crossings; long-range couplings (C_3/R^3, C_6/R^6, etc.) are neglected and near-resonant excitation-transfer processes where such couplings are important are not treated.[36] Hence A-core states are coupled with B-core states but A-core states are not coupled with other A-core states; likewise, B-core states are not coupled with other B-core states. The small-angle crossings between some pairs of A-core states in the region of the minima occur at smaller distances than do the crossings with the repulsive curves; they are expected to have little effect on the AI cross sections (this would not be the case if nonadiabatic coupling to the continuum states dominated). These assumptions are expected to be good for low-energy scattering.

Since a number of potential curves and crossings are usually important in a collision, interference effects are expected to tend to cancel out and were consequently neglected. Also, the integrated cross section, which is the subject of primary interest, is not usually sensitive to interference. The transition regions associated with various pairs of potential curves are considered to be independent, with the transition probability depending only on the potentials in the vicinity of the crossing. A further approximation to determine the crossing probabilities, use of the Landau-Zener (LZ) formula,[37] was checked by Numerov integration of the two-state coupled equations, with semiclassical separation of the in-out waves, and found to be good for the present parameters, but it is not essential to the model. The LZ probability for staying on the same diabatic curve in a single pass through a crossing at R_x is given, in the case of radial coupling, by

$$p = e^{-2\pi\gamma_l}, \tag{3}$$

where

$$\gamma_l = \frac{|V_{12}(R_x)|^2}{v_R(R_x)\,|(d/dR)(V_{11}-V_{22})|_{R=R_x}} \tag{4}$$

(atomic units are used), with the velocity $v_R(R_x)$ determined by

$$\tfrac{1}{2}\mu v_R(R_x)^2 = E - V_{11}(R_x) - (l+\tfrac{1}{2})^2/(2\mu R_x^2)\,. \tag{5}$$

In the case of angular coupling V_{12} is replaced by $\omega\Omega_{12}$, where Ω_{12} is the matrix element $\langle\psi_1|L_\perp|\psi_2\rangle$, and the angular velocity is given by[38]

$$\omega = (l+\tfrac{1}{2})/(\mu R_x^2)\,. \tag{6}$$

The formulas derived in the following section involve p's for many different curve crossings but are not restricted to usage of the LZ expression. The transition probability associated with the ith repulsive curve and the ath attractive curve is designated p_{ia}—indices i, j, and k are used for repulsive curves, and indices a, b, and c for

attractive curves. By $i<j$ ($a<b$) we shall mean that i (a) is energetically lower than j (b).

B. Internal transition matrices

We first consider the case of a single attractive curve a being crossed by a number, say n_r, of repulsive curves as shown in Fig. 1. Then the following question must be answered: If the system is initially on curve i, with upward (R decreasing) or downward (R increasing) motion *toward* curve a specified, what is the probability that, as a result of the interaction with a, the system will be on curve j, moving upward or downward *away* from a, or dissociating along attractive curve a? To answer this question four $n_r \times n_r$ square matrices and two $1 \times n_r$ row matrices, where the subscripts denote members of the set of repulsive curves, will be defined:

T^a_{ji} = Probability of $i_{\text{up}} \rightarrow j_{\text{up}}$ [Fig. 1(a)], upward transmission;

$\bar{T}^a_{ji}$ = Probability of $i_{\text{down}} \rightarrow j_{\text{down}}$ [Fig. 1(d)], downward transmission;

R^a_{ji} = Probability of $i_{\text{up}} \rightarrow j_{\text{down}}$ [Fig. 1(b)], downward reflection;

$\bar{R}^a_{ji}$ = Probability of $i_{\text{down}} \rightarrow j_{\text{up}}$ [Fig. 1(e)], upward reflection;

D^a_i = Probability of $i_{\text{up}} \rightarrow a_{\text{dissoc.}}$ [Fig. 1(c)], upward dissociation;

$\bar{D}^a_i$ = Probability of $i_{\text{down}} \rightarrow a_{\text{dissoc.}}$ [Fig. 1(f)], downward dissociation.

It should be emphasized that these probabilities describe interaction with curve a only. With the above notation the inverse "transition" may be obtained by reversing the directions both of the arrow and of the directional subscripts (up $\rightleftharpoons$ down, dissociation $\rightleftharpoons$ association). Application of the principle of microscopic reversibility, which can be easily demonstrated to hold, shows $T^a_{ji} = \bar{T}^a_{ij}$, $R^a_{ji} = R^a_{ij}$, and $\bar{R}^a_{ji} = \bar{R}^a_{ij}$. Hence matrices $\underline{R}^a$ and $\underline{\bar{R}}^a$ are symmetric but $\underline{T}^a$ and $\underline{\bar{T}}^a$ will be shown to be asymmetric. The following conservation relations can also be proved:

$$\sum_{j=1}^{n_r} (T^a_{ji} + R^a_{ji}) + D^a_i = 1 \tag{7}$$

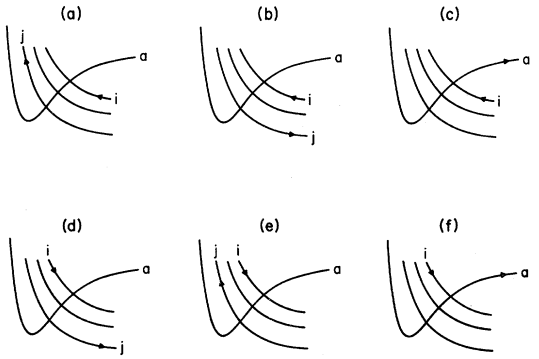

FIG. 1. Pictoral representation of the internal transitions described by the probability matrices defined in the text. (a) Upward transmission T^a_{ji}; (b) downward reflection R^a_{ji}; (c) upward dissociation D^a_i; (d) downward transmission $\bar{T}^a_{ji}$; (e) upward reflection $\bar{R}^a_{ji}$; (f) downward dissociation $\bar{D}^a_i$.

and

$$\sum_{j=1}^{n_r} (\bar{T}^a_{ji} + \bar{R}_{ji}) + \bar{D}^a_i = 1, \tag{8}$$

for any i.

First consider the case that a is open such that dissociation along a is energetically possible. Then if a given transition is possible at all it can be attained by only a specific path. The results for the transition matrices are

$$T^{a(\text{op})}_{ji} = \begin{cases} p_{ia} & \text{for } i=j, \\ 0 & \text{for } i<j, \\ (1-p_{ja})\left(\prod_{k=j+1}^{i-1} p_{ka}\right)(1-p_{ia}) & \text{for } i>j, \end{cases} \tag{9}$$

$$\underline{\bar{T}}^{a(\text{op})} = \underline{\tilde{T}}^{a(\text{op})}, \tag{9a}$$

$$R^{a(\text{op})}_{ji} = R^{a(\text{op})}_{ij} = (1-p_{ja})\left(\prod_{k=i}^{j-1} p_{ka}\right)\left(\prod_{k=1}^{i-1} p_{ka}\right)^2 \times (1-p_{ia}) \quad \text{for } i \leq j, \tag{10}$$

$$\underline{\bar{R}}^{a(\text{op})} = \underline{0}, \tag{11}$$

$$D^{a(\text{op})}_i = \left(\prod_{k=i}^{n_r} p_{ka}\right)\left(\prod_{k=1}^{i-1} p_{ka}\right)^2 (1-p_{ia}), \tag{12}$$

and

$$\bar{D}^{a(\text{op})}_i = \left(\prod_{k=i+1}^{n_r} p_{ka}\right)(1-p_{ia}). \tag{13}$$

The following conventions are used with the product symbol: The product proceeds from right to left, and if the upper limit is smaller than the

lower limit the product is set to unity.

Next, consider the case that curve a is closed, but the lowest n_{r0}, $n_{r0} \leq n_r$, crossings of repulsive curves with a are energetically accessible. The row matrices $\underline{D}^{a(\mathrm{cl})}$ and $\overline{\underline{D}}^{a(\mathrm{cl})}$ vanish, but the closure makes possible an infinite series of contributions to $\underline{T}^{a(\mathrm{cl})}$, $\underline{R}^{a(\mathrm{cl})}$, and $\overline{\underline{R}}^{a(\mathrm{cl})}$ with the same contribution as in the case of a open being the first term. The same sum, which takes the form of a simple geometric series, appears in all the formulas and for conciseness will be designated

$$G(p_a) = \sum_{m=0}^{\infty} \left(\prod_{k=1}^{n_{r0}} p_{ka} \right)^{2m} = \left[1 - \left(\prod_{k=1}^{n_{r0}} p_{ka} \right)^2 \right]^{-1} . \tag{14}$$

The results are

$$T_{ji}^{a(\mathrm{cl})} = \overline{T}_{ij}^{a(\mathrm{cl})} = \begin{cases} p_{ia} + (1-p_{ia}) \left(\prod_{k=i+1}^{n_{r0}} p_{ka} \right)^2 p_{ia} \left(\prod_{k=1}^{i-1} p_{ka} \right)^2 (1-p_{ia}) G(p_a) & \text{for } i=j, \\ (1-p_{ja}) \left(\prod_{k=j+1}^{i-1} p_{ka} \right) (1-p_{ia}) G(p_a) & \text{for } i>j, \\ (1-p_{ja}) \left(\prod_{k=j+1}^{n_{r0}} p_{ka} \right)^2 \left(\prod_{k=i}^{j} p_{ka} \right) \left(\prod_{k=1}^{i-1} p_{ka} \right)^2 (1-p_{ia}) G(p_a) & \text{for } i<j, \end{cases} \tag{15}$$

$$R_{ji}^{a(\mathrm{cl})} = R_{ij}^{a(\mathrm{cl})} = (1-p_{ja}) \left(\prod_{k=i}^{j-1} p_{ka} \right) \left(\prod_{k=1}^{i-1} p_{ka} \right)^2 (1-p_{ia}) G(p_a) \quad \text{for } i \leq j , \tag{16}$$

and

$$\overline{R}_{ji}^{a(\mathrm{cl})} = \overline{R}_{ij}^{a(\mathrm{cl})} = (1-p_{ja}) \left(\prod_{k=j+1}^{n_{r0}} p_{ka} \right)^2 \left(\prod_{k=i+1}^{j} p_{ka} \right) (1-p_{ia}) G(p_a) \quad \text{for } i \leq j . \tag{17}$$

In the present formulation, ionization in the electronic continuum can be taken into account by the matrices $\underline{T}$, $\underline{R}$, and $\underline{D}$ describing the influence of attractive pseudocurves in the continuum. As a simplification it will be assumed that the only transition occurring in the continuum is emission of an electron; i.e., transitions between repulsive curves are not allowed in this region. In general one might use a pseudocurve for each vibrational-rotational level of the molecular ion plus more for the dissociative continuum, but the above simplification makes a single pseudocurve suffice. If the final state of the ion is left unspecified, two quantities, p_j^{AI} and p_j^{DI}, give the associative and dissociative ionization probabilities for a given repulsive curve j crossing into the electronic continuum; the matrices can be written

$$T_{ji}^{(\mathrm{cont})} = p_j^{\mathrm{AI}} \delta_{ji} , \tag{18}$$

$$D_j^{(\mathrm{cont})} = p_j^{\mathrm{DI}} , \tag{19}$$

and

$$R_{ji}^{(\mathrm{cont})} = (1 - p_j^{\mathrm{AI}} - p_j^{\mathrm{DI}}) \delta_{ji} . \tag{20}$$

Here $\underline{T}$ and $\underline{D}$ represent scattering into associative and dissociative ionization channels, respectively. The ionization probabilities can be written in terms of two phase shifts as follows (omitting the subscripts for brevity):

$$p^{\mathrm{AI}} = e^{-2\eta_2} - e^{-2(2\eta_1+\eta_2)} , \tag{21}$$

$$p^{\mathrm{DI}} = 1 - e^{-2\eta_2} + e^{-2(2\eta_1+\eta_2)} - e^{-4(\eta_1+\eta_2)} , \tag{22}$$

and

$$p_T^{\mathrm{I}} = p^{\mathrm{AI}} + p^{\mathrm{DI}} = 1 - e^{-4(\eta_1+\eta_2)} . \tag{23}$$

A simple way to obtain this form is by solution of the differential equation

$$dp/dR = \gamma(R)(1-p) , \tag{24}$$

where $\gamma(R) \simeq \Gamma(R)/v(R)$ in terms of the autoionization width and relative velocity. The ionizing transition will be assumed to obey the Franck-Condon principle. The phase shifts η_1 and η_2 can be calculated in the JWKB approximation as components of the imaginary part of the complex phase shift resulting from scattering by the complex local potential,[39] $V_j(R) - \frac{1}{2} i \Gamma_j(R)$. The results are

$$\eta_1 = \eta_0^{(-)}(R_c)[1 - \theta(R_c - R_d)] + \mathrm{Im} \int_{R_c}^{\mathrm{Max}(R_c, R_d)} K(R)\, dR \tag{25}$$

and

$$\eta_2 = \eta_0^{(-)}(R_c)\theta(R_c - R_d) + \mathrm{Im} \int_{\mathrm{Max}(R_c, R_d)}^{\infty} K(R)\, dR , \tag{26}$$

where R_c is the classical turning point on curve j, R_d is defined by

$$V_j(R_d) - V_+(R_d) = E - V_+(\infty) \tag{27}$$

with V_+ the potential energy of the molecular ion and all energies measured from a common reference point,

$$\theta(R) = \begin{cases} 1 & \text{if } R \geq 0 \\ 0 & \text{if } R < 0, \end{cases} \tag{28}$$

$$K(R) = \{2\mu[E - U_l(R) + \tfrac{1}{2}i\Gamma(R)]\}^{1/2}, \tag{29}$$

$$U_l(R) = V_j(R) + (l+\tfrac{1}{2})^2/(2\mu R^2), \tag{30}$$

and

$$\eta_0^{(-)}(R) = -\tfrac{1}{6}(2\mu)^{1/2}\Gamma^{3/2}(U_l' - \tfrac{1}{2}\Gamma')/(U_l'^2 + \tfrac{1}{4}\Gamma'^2) \tag{31}$$

(denoting differentiation with respect to R by a prime). It is assumed that

$$V_j(R) - V_+(R) \lesssim E - V_+(\infty) \quad \text{for } R \gtrsim R_d. \tag{32}$$

Defining R_x as the outermost distance at which $V_j(R) = V_+(R)$, it should be noted that $\Gamma(R) = 0$ and $\mathrm{Im}K(R) = 0$ for $R > R_x$. Writing ImK in the more convenient form

$$\mathrm{Im}K = \tfrac{1}{2}\mu^{1/2}\Gamma/\{[(E - U_l)^2 + \tfrac{1}{4}\Gamma^2]^{1/2} + E - U_l\}^{1/2} \tag{33}$$

and assuming Γ is not too large, it is clear that

$$\eta_1 \simeq \tfrac{1}{2}\int_{R_c}^{\mathrm{Max}(R_c, R_d)} \frac{\Gamma(R)}{v_l(R)}\,dR \tag{34}$$

and

$$\eta_2 \simeq \tfrac{1}{2}\int_{\mathrm{Max}(R_c, R_d)}^{\infty} \frac{\Gamma(R)}{v_l(R)}\,dR, \tag{35}$$

where $v_l(R)$ is the relative velocity on curve j at internuclear distance R.

All of the asymptotically closed channels can be combined into a single effective potential (this will allow a simpler form for the equations in Sec. II C), keeping in mind that the probability matrices are defined such that products should be time ordered with earliest times to the right. We denote the number of open attractive curves by n_{ao} and the total number of attractive curves by n_a. The matrices $\underline{\mathcal{T}}^b$, $\underline{\bar{\mathcal{R}}}^b$, and $\underline{\mathcal{R}}^b$, where $n_{ao} \leq b \leq n_a$, are defined analogously to $\underline{T}^a$, $\underline{\bar{R}}^a$, and $\underline{R}^a$ to describe the effects of all the closed channels $n_{ao} < a \leq b$ together. The results are given by the following recursion relations:

$$\underline{\mathcal{T}}^{n_{ao}} = \underline{1}, \quad \underline{\mathcal{R}}^{n_{ao}} = \underline{\bar{\mathcal{R}}}^{n_{ao}} = \underline{0}, \tag{36}$$

$$\underline{\mathcal{T}}^b = \underline{T}^b(\underline{1} - \underline{\bar{\mathcal{R}}}^{b-1}\underline{R}^b)^{-1}\underline{\mathcal{T}}^{b-1}, \tag{37}$$

$$\underline{\mathcal{R}}^b = \underline{\mathcal{R}}^{b-1} + \underline{\tilde{\mathcal{T}}}^{b-1}\underline{R}^b(\underline{1} - \underline{\bar{\mathcal{R}}}^{b-1}\underline{R}^b)^{-1}\underline{\mathcal{T}}^{b-1}, \tag{38}$$

$$\underline{\bar{\mathcal{R}}}^b = \underline{\bar{R}}^b + \underline{T}^b(\underline{1} - \underline{\bar{\mathcal{R}}}^{b-1}\underline{R}^b)^{-1}\underline{\bar{\mathcal{R}}}^{b-1}\underline{\tilde{T}}^b. \tag{39}$$

The matrices describing the ionization channels, indexed $n_a + 1$, can also be included in this effective potential if they are closed with respect to dissociation. The effective potential will be formally treated as just the $(n_{ao}+1)$th and last curve making the following identifications:

$$\underline{\mathcal{T}}^{n_a+1} \to \underline{T}^{n_{ao}+1}, \tag{40}$$

$$\underline{\mathcal{R}}^{n_a+1} \to \underline{R}^{n_{ao}+1}. \tag{41}$$

C. Reaction probabilities

The cross section for any excitation transfer between open channels and for ionization via any repulsive curve whose crossing with the electronic continuum is energetically accessible can now be determined from the above matrices. For this purpose two column matrices will be defined to give the initial scattering conditions. There are two cases to be considered, a repulsive initial state and an attractive initial state, as shown in Fig. 2. Since the problem has been indexed in terms of the repulsive curves, we wish to know the initial flux on these curves; to this end $\underline{X}$ will be defined to give the effective initial flux upward, and $\underline{\bar{X}}$ the effective initial flux downward. In the case where the incoming state has repulsive curve ι the result is obviously just

$$X_j = \delta_{j,\iota}, \tag{42}$$

$$\underline{\bar{X}} = \underline{0}. \tag{43}$$

In the case where the incoming state has attractive curve α, the principle of reversibility shows that the repulsive curves are first given flux according

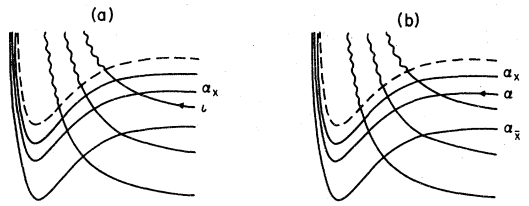

FIG. 2. Pictoral definition of the indices associated with the initial conditions for the case (a) that the incoming state has repulsive curve ι and the case (b) that the incoming state has attractive curve α. The continuum limit is shown schematically as a dashed line and the diabatic states in the continuum as wavy lines.

to the transposes of the dissociation matrices $\underline{D}^{\alpha}$ and $\overline{\underline{D}}^{\alpha}$,

$$\underline{X}=\tilde{\underline{D}}^{\alpha}, \tag{44}$$

$$\overline{\underline{X}}=\tilde{\underline{D}}^{\alpha}. \tag{45}$$

If the initial state is repulsive, we let $\alpha=0$ in the formulas below. Two additional indices associated with the incoming state will be defined: α_x, the lowest attractive state above the incoming state asymptotically, and $\alpha_{\overline{x}}$, the highest attractive state below the incoming state asymptotically. The associative ionization probabilities are then given by

$$\underline{P}^{\mathrm{AI}}=\left(\prod_{a=\alpha_x}^{n_{ao}+1}\underline{T}^{a}\right)\underline{X}, \tag{46}$$

and the dissociative ionization probabilities by

$$\underline{P}^{\mathrm{DI}}=\underline{D}^{n_{ao}+1}\left(\prod_{a=\alpha_x}^{n_{ao}}\underline{T}^{a}\right)\underline{X}, \tag{47}$$

where the jth component of the column matrix gives the probability of ionization from the jth repulsive state. It should be remembered that index $n_{ao}+1$ refers to the *pseudostate* representing the effects of all the closed channels and the ionization channels. The total ionization probability is

$$P_T^{\mathrm{I}}=\sum_{j=1}^{n_r}(P_j^{\mathrm{AI}}+P_j^{\mathrm{DI}}). \tag{48}$$

The excitation-transfer probability is derived separately for the cases that the *final* atomic states dissociate from repulsive or attractive potential curves.

First consider a repulsive final state. There are two contributions in the present formulation: An initial upward trajectory may be reflected by some higher state and penetrate downward to dissociation, and an initial downward trajectory may penetrate to dissociation (this contribution applies only if the incoming state is attractive). The result is given by

$$\underline{P}^{\mathrm{ET}(r)}=\left[\sum_{b=\alpha_x}^{n_{ao}+1}\left(\prod_{a=1}^{b-1}\underline{T}^{a}\right)^{\dagger}\underline{R}^{b}\left(\prod_{a=\alpha_x}^{b-1}\underline{T}^{a}\right)\right]\underline{X} + \left(\prod_{a=1}^{\alpha_{\overline{x}}}\underline{T}^{a}\right)^{\dagger}\overline{\underline{X}}, \tag{49}$$

where a superscript † has been used to designate the transpose of a matrix product. The element $P_j^{\mathrm{ET}(r)}$ is the probability of excitation transfer from the initial state to the atomic state to which the jth repulsive curve dissociates. Similar contributions are made to excitation transfer in the case that the final dissociating state is attractive. An additional contribution is due to the possibility that the system on the upward trajectory may dissociate without downward reflection. One more term is added to allow for the possibility of direct elastic scattering involving only the initial potential curve. The result can be written for the open attractive state c,

$$P_c^{\mathrm{ET}(a)}=\left[\overline{\underline{D}}^{c}\sum_{b=\mathrm{Max}(\alpha_x,c+1)}^{n_{ao}+1}\left(\prod_{a=c+1}^{b-1}\underline{T}^{a}\right)^{\dagger}\underline{R}^{b}\left(\prod_{a=\alpha_x}^{b-1}\underline{T}^{a}\right)+\underline{D}^{c}\left(\prod_{a=\alpha_x}^{c-1}\underline{T}^{a}\right)\theta_{c,\alpha_x}\right]\underline{X}+\left[\overline{\underline{D}}^{c}\left(\prod_{a=c+1}^{\alpha_{\overline{x}}}\underline{T}^{a}\right)^{\dagger}\theta_{\alpha_{\overline{x}},c}\right]\overline{\underline{X}}+\left(\prod_{k=1}^{n_r}p_{kc}\right)^{2}\delta_{c,\alpha}, \tag{50}$$

where $\delta_{i,j}$ is the Kronecker delta and

$$\theta_{a,b}=\begin{cases}1 & \text{if } a\geq b\\ 0 & \text{if } a<b\end{cases}. \tag{51}$$

Finally, we shall show that a small modification of the above formulas for the reaction probabilities can take into account a barrier in the incoming channel. The probability p_t of tunneling through a potential barrier is given in the JWKB approximation by[40]

$$p_t=\frac{4}{(2\zeta+1/2\zeta)^2}, \tag{52}$$

with

$$\zeta=\exp\left(\int_{R_1}^{R_2}\kappa(R)\,dR\right), \tag{53}$$

where

$$\kappa(R)=\{2\mu[U_l(R)-E]\}^{1/2}, \tag{54}$$

$$U_l(R)=V(R)+(l+\tfrac{1}{2})^2/(2\mu R^2), \tag{55}$$

$$\kappa(R_1)=\kappa(R_2)=0, \tag{56}$$

and $\kappa(R)$ is real for $R_1<R<R_2$. We assume that there are no crossings with the initial curve at distances larger than R_2. Denoting the nonreactive (elastic) probability given by some component of Eq. (49) or (50) by P_e, and the reactive cross section for channel ν given by some component of Eqs. (46)–(50) by $P_{r\nu}$, the corresponding probabilities, taking the barriers into account, are

given by

$$P_e^t = (1-p_t) + p_t P_e p_t + p_t P_e (1-p_t) P_e p_t + \cdots$$
$$= 1 - p_t + \left(\frac{p_t}{1 - P_e + p_t P_e}\right) P_e p_t \tag{57}$$

and

$$P_{rv}^t = P_{rv} p_t + P_{rv}(1-p_t) P_e p_t + \cdots$$
$$= \left(\frac{p_t}{1 - P_e + p_t P_e}\right) P_{rv} . \tag{58}$$

It is easy to see that

$$P_e^t + \sum_v P_{rv}^t = 1 \tag{59}$$

if

$$P_e + \sum_v P_{rv} = 1 . \tag{60}$$

In the case where there is no barrier or in the case where the scattering energy exceeds the barrier height we shall take $p_t = 1$ (the discontinuity in p_t as $\zeta \to 1$ is of little concern since usually $\zeta \gg 1$ in our applications).

III. CROSS SECTIONS

The reaction probabilities of Sec. II C are related to cross sections for collisions with impact parameter $b = (l + \frac{1}{2})/k$ by

$$Q(l) = (\pi/k^2)(2l+1) P(l) , \tag{61}$$

where l is the orbital angular momentum and k is the asymptotic wave number. In the usual partial-wave expansion, the integrated cross section is written

$$Q = \sum_{l=0}^{l_x} Q(l) , \tag{62}$$

where l_x is the largest integral value of l such that v_R given by Eq. (5) is real at some crossing under consideration. In the case of scattering of two identical spin-s particles,

$$Q = \lambda(Q^g_{\text{even } l} + Q^u_{\text{odd } l}) + (1-\lambda)(Q^g_{\text{odd } l} + Q^u_{\text{even } l}) , \tag{63}$$

where

$$\lambda = \begin{cases} (s+1)/(2s+1) & \text{for } s \text{ integral} \\ s/(2s+1) & \text{for } s \text{ half-integral} , \end{cases} \tag{64}$$

$g(u)$ indicates the cross section calculated with the gerade (ungerade) potential curves, and "even l" ("odd l") implies use of Eq. (62) with only even (odd) values of l included. In the case of nonidentical particles with equal nuclear charge or if nuclear statistics are neglected, the result is the simple average

$$Q = \tfrac{1}{2}(Q^g + Q^u) , \tag{65}$$

with all integral values of l included in Eq. (62). In preliminary reports of this work[41] the partial-wave parameter l was taken as quantized, but the stepwise increase in l_x as the scattering energy increased led to sharp structure in some of the integrated cross sections as a function of energy. This incidental structure tended to obscure the more interesting effects owing to thresholds, curve crossings, etc., and may be expected to be smoothed in a quantum-mechanical calculation. Consequently it was considered better to treat l (or b) as continuous and take the integrated cross section as

$$Q = \tfrac{1}{2}\left(\int_0^{l_x} Q^g(l)\, dl + \int_0^{l'_x} Q^u(l)\, dl\right), \tag{66}$$

where l_x (l'_x) is the value of l which makes v_R vanish at the last accessible crossing for the g (u) curves. It should be noted that although the impact parameter is treated as continuous, assumption of a straight-line trajectory is not good at the low scattering energies under consideration and is not made. The integral of Eq. (66) was evaluated by Gauss-Legendre quadrature. To obtain the integral accurately with the smallest possible number of quadrature points, it was found useful to perform the quadrature in segments,

$$Q = \tfrac{1}{2}\left(\sum_{i=1}^{m} \int_{l_{i-1}}^{l_i} Q^g(l) + \sum_{i=1}^{m'} \int_{l'_{i-1}}^{l'_i} Q^u(l)\right), \tag{67}$$

where $l_0 = 0$, $l_m = l_x$, and l_i is the value of l for which the ith crossing is just accessible; i.e., there is a segment for each curve crossing.

In general the observable cross section is a weighted average for scattering on more than one initial potential curve. In a collision of $He^*(n^3L)$ with $He(1\,^1S)$ the particles can interact with triplet, gerade or ungerade, $\Lambda = 0(\Sigma), 1(\Pi), \ldots, L$ symmetry, and the observable cross section (neglecting nuclear statistics) is given by

$$Q(n^3L) = \frac{1}{2L+1} \sum_{\Lambda=0}^{L} \tfrac{1}{2} g_\Lambda [Q(^3\Lambda_g\, n^3L) + Q(^3\Lambda_u\, n^3L)] , \tag{68}$$

where $g_\Lambda = 1$ for Σ states and $= 2$ otherwise. In the present calculations the diabatic representation of Paper I, with the long-range coupling deduced from the adiabatic potential curves, is used.[12] Since angular couplings were shown to be negligible for the transitions under consideration the terms in the sum over Λ in Eq. (68) are nonzero only for $\Lambda \leq \text{Min}(L, L')$ if the final state is

$He^*(n'^3L') + He(1\,^1S)$. In addition, the neglect of angular coupling means that the couplings are block diagonal with respect to each molecular symmetry, and the matrix calculations of cross sections for the various molecular symmetries are independent. Otherwise, two larger matrix calculations would have to be performed, one for the gerade states and a second for the ungerade states. In the case of ionization, all terms with $\Lambda \leq L$ contribute if the angular momentum of the ejected electron is left unspecified.

The autoionization widths $\Gamma(R)$ corresponding to the wave functions of Paper I have not been calculated so far. The width is expected to be large near the crossing of the diabatic curve into the ionization continuum and its integral over the trajectory is assumed to be sufficiently large that ionization always occurs when the continuum is penetrated. Only the total (i.e., the sum of associative and dissociative) ionization cross sections are presented in this paper. This approximation will be discussed further in Sec. V.

IV. RESULTS AND COMPARISON WITH EXPERIMENT

As shown in Secs. II and III, the observable ionization cross section is a statistical average of cross sections owing to the potential curves of different symmetries arising from a given excited atomic level, each of which is in turn a sum of contributions from the various repulsive curves of that symmetry which cross into the ionization continuum. Both of these effects can yield broad structural features in the observable integrated cross section. In addition, thresholds and closed-channel resonances tend to introduce narrower structures. The outstanding features of the cross sections are easily explainable in terms of the potential curves of Paper I. We shall look first at examples of contributions of particular diabatic curves crossing into the continuum.

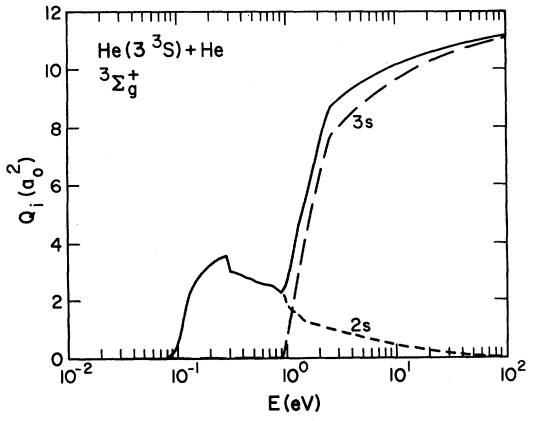

FIG. 3. Contribution of $^3\Sigma_g^+$ scattering to the ionization cross section for $He(3\,^3S) + He(1\,^1S)$ collisions. The contribution of each repulsive diabatic curve crossing into the continuum and the total contribution of all curves of this symmetry are shown separately. The integrated cross sections are plotted in units of a_0^2 ($=0.280\times10^{-16}$ cm^2) vs energy (in eV) on a logarithmic scale.

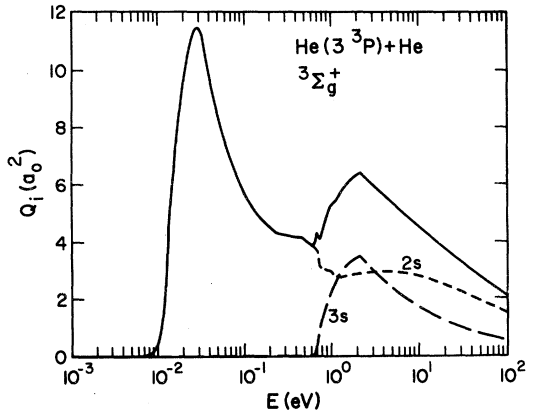

FIG. 4. Contribution of $^3\Sigma_g^+$ scattering to the ionization cross section for $He(3\,^3P) + He(1\,^1S)$ collisions. The cross section is normalized to unit flux on the $^3\Sigma$ curves; i.e., it has not yet been multiplied by the factor $g_\Lambda/(2L+1)$ in Eq. (68), but has been multiplied by the factor $\frac{1}{2}$.

The cross section $\frac{1}{2}Q(^3\Sigma_g^+\ 3\,^3S)$ is shown in Fig. 3 along with its components. The $^3\Sigma_g^+$ 3s diabatic curve is repulsive and close collisions cannot occur at very low energies, resulting in the first threshold at about 0.08 eV. Tunneling yields the more gradual onset at this energy rather than a sharp onset at 0.15 eV which is the barrier height

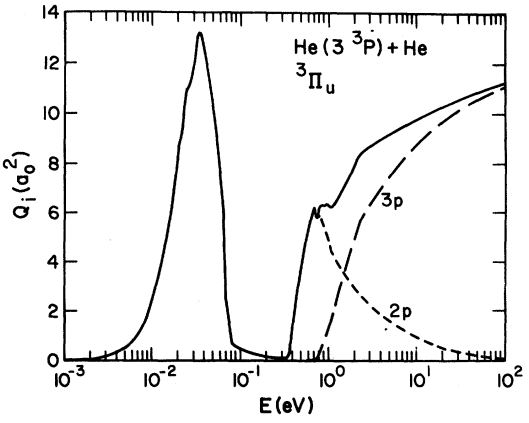

FIG. 5. Contribution of $^3\Pi_u$ scattering to the ionization cross section for $He(3\,^3P) + He(1\,^1S)$ collisions. The cross section is normalized to unit flux on the $^3\Pi$ curves.

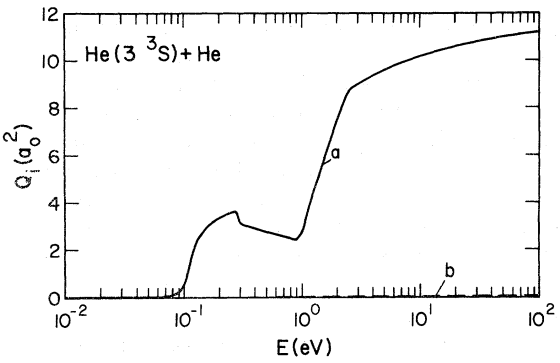

FIG. 6. Ionization cross section for $He(3\,^3S)+He(1\,^1S)$ collisions. The component contributions [see Eq. (68)] are designated in this and the following figures as follows: $a=\,^3\Sigma_g^+$, $b=\,^3\Sigma_u^+$, $c=\,^3\Pi_g$, $d=\,^3\Pi_u$, and $e=\,^3\Delta_g$.

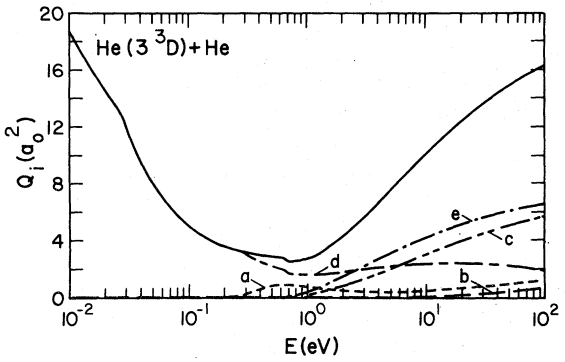

FIG. 8. Ionization cross section for $He(3\,^3D)+He(1\,^1S)$ collisions. See Fig. 6 for notation.

in the adiabatic curve. The crossing of the $2s$ diabatic curve into the continuum at 0.07 eV is already accessible at energies required to penetrate the barrier; the next crossing into the continuum, by the $3s$ diabatic curve, occurs at 0.93 eV and results in a second threshold. Clearly, the most direct possible path to ionization at low scattering energies is from the $^3\Sigma_g^+$ $2s$ curve with the trajectory $3s \rightarrow 3p \rightarrow 2s \rightarrow i$ (a diabatic curve is denoted by the Rydberg electron), whereas at higher collision energies ionization via the initial $3s$ curve is possible with no intermediate transitions required. The dip in the cross section at about 0.30 eV is a typical structure and very easy to explain. This particular feature is due to the opening of the $3p$ inelastic channel and is required for conservation of flux. The $^3\Sigma_g^+$ $3d$ diabatic curve also makes a contribution to ionization at collision energies in the range 1.1–1.4 eV because of the closed channels, but the contribution is at most only about $0.05a_0^2$, too small to be shown in Fig. 3. The other repulsive diabatic curves make negligible contributions. In general, a diabatic curve in the continuum which is accessible only because of the closed channels yields a relatively small cross section, but the structural feature is sometimes still interesting because it is narrow, i.e., a type of resonance. This effect could possibly be observed as an enhancement of the cross section for associative ionization into certain higher-lying vibrational levels.

Two more examples are shown in Figs. 4 and 5, the $^3\Sigma_g^+$ and $^3\Pi_u$ contributions to ionization in collisions of $He(3\,^3P)$ with the ground-state atom. The $^3\Sigma_g^+$ $2s$ crossing into the continuum lies lower than the $3\,^3P$ asymptotic limit and the $^3\Sigma_g^+$ $3p$ curve is mainly attractive, but there is still a very low energy threshold in the reaction arising from the small barrier in the $3p$ curve. The small cusps in the region 0.5–1.0 eV of the cross section result from the opening of new inelastic and ionization channels. The main contribution to the $2s$ component of ionization comes from the path $3p \rightarrow 2s \rightarrow i$, but a secondary broad maximum in the $2s$

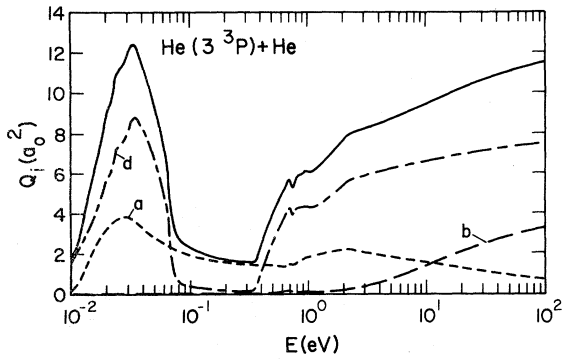

FIG. 7. Ionization cross section for $He(3\,^3P)+He(1\,^1S)$ collisions. See Fig. 6 for notation.

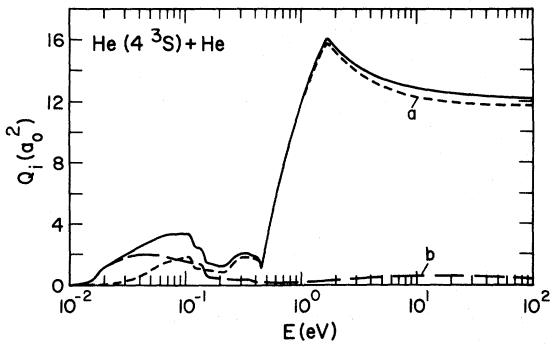

FIG. 9. Ionization cross section for $He(4\,^3S)+He(1\,^1S)$ collisions. See Fig. 6 for notation.

contribution occurs around 4 eV owing to paths like $3p \to 3s \to 4f \to 2s \to i$. A second large $^3\Sigma_g^+$ contribution to the ionization cross section comes as the crossing of the $3s$ curve into the continuum becomes accessible. The $^3\Pi_u$ contribution to $3\,^3P$ ionization, shown in Fig. 5, is interesting because an initial repulsive curve still provides a large contribution to the low-energy ionization cross section. The $2p$ contribution has two large peaks. The low-energy peak (~0.034 eV) results from following the $3p$ adiabatic curve past the $3d$ avoided crossing with some tunneling through the barrier—in diabatic terminology the path is $3p \to 3d \to 2p \to i$. The higher-energy peak (~0.80 eV) results from staying on the $3p$ diabatic curve through the crossing with the $3d$ curve, with the main path being $3p \to 4d \to 2p \to i$. The valley in between occurs when the $3p$-$3d$ crossing probability is high but the $4d$ curve is not yet energetically accessible. At still higher energies the direct $3p$ contribution becomes dominant.

The observable ionization cross sections, and their components in Eq. (68), are presented in Figs. 6–11 for collisions of He($3\,^3S$), He($3\,^3P$), He($3\,^3D$), He($4\,^3S$), He($4\,^3P$), and He($4\,^3D$), respectively, with the ground-state helium atom. The contributions of the various molecular symmetries are labeled as follows: $a = {}^3\Sigma_g^+$, $b = {}^3\Sigma_u^+$, $c = {}^3\Pi_g$, $d = {}^3\Pi_u$, and $e = {}^3\Delta_g$. The $^3\Delta_u$ diabatic curves arising from the $3d$ and $4d$ atoms have no crossings with other diabatic states of this symmetry and no pathway to the continuum; therefore they make no contribution within the present model. A few comments will be made about the main features of these cross sections.

The $^3\Sigma_g^+$ contribution to $3\,^3S$ ionization has already been discussed. The $^3\Sigma_u^+$ contribution is so small that it is insignificant in Fig. 6; the smallness of this cross section is a result of the large coupling matrix elements between the $2p$ and nd states, which make it very difficult to penetrate through the Rydberg series. The main contributions to $3\,^3P$ ionization have already been discussed in connection with Figs. 4 and 5. Only at rather high energies does the $^3\Sigma_u^+$ contribution become significant. There is no mechanism for a $^3\Pi_g$ contribution; thus its flux is lost as far as $3\,^3P$ ionization is concerned. The He($3\,^3D$) ionization cross section displays a rather typical behavior. The cross section is decreasing at low energy, reaches a minimum, and then begins to increase again. The decreasing cross section at low energies is characteristic of scattering with initial attractive curves, and the increasing cross section at higher energies is characteristic of initial repulsive curves. At very low energies the classical turning point on a repulsive curve is outside the required crossings, whereas at sufficiently high energies the system can stay on a repulsive diabatic curve and penetrate the Rydberg series as if it did not exist. In the present case low-energy ionization occurs via the $^3\Pi_u$ curves; since there are no barriers in the non-Σ diabatic curves the cross section continues to increase with decreasing collision energy even at very low energies. This situation may be contrasted to that of the $3\,^3P$ cross section. Virtually all of the $^3\Pi_u$ contribution to the $3\,^3D$ ionization cross section comes from the $2p$ diabatic curve, since at energies high enough for the crossing of the $3p$ curve with the continuum to be accessible the crossing of the $3d$ and $3p$ curves is very easily made. At the higher energies all the various sets of potential curves tend to contribute to the cross section. At sufficiently high energies (not shown) the ionization cross section must begin to decrease again since the particles will not spend enough time in the continuum for ionization to occur; this will be the case when $v(R)$ becomes large enough that the integrals in Eqs. (34) and (35) become small.

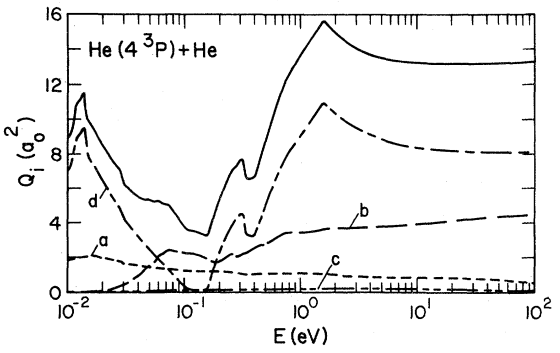

FIG. 10. Ionization cross section for He($4\,^3P$) + He($1\,^1S$) collisions. See Fig. 6 for notation.

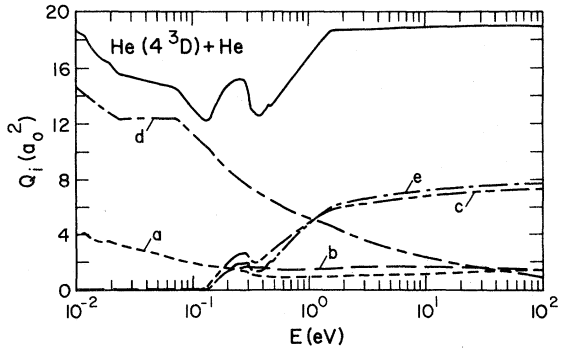

FIG. 11. Ionization cross section for He($4\,^3D$) + He($1\,^1S$) collisions. See Fig. 6 for notation.

The ionization cross sections for the $n=4$ levels at low energies tend to be somewhat larger than the corresponding cross sections for the $n=3$ levels for two reasons: the potential barriers, if present, are lower, and the higher initial total energy makes more crossings accessible and the higher crossings have greater crossing probabilities. The $4\,^3S$ ionization cross section is shown in Fig. 9. The $^3\Sigma_u^+$ contribution is somewhat larger for $4\,^3S$ than for $3\,^3S$ since, for the $4\,^3S$, the rather strongly avoided $2p$-$3d$ crossing does not have to be made. The behavior of the $4\,^3P$ ionization cross section shown in Fig. 10 is qualitatively similar to that of the $3\,^3P$. The three relative maxima in the $^3\Pi_u$ contribution can be ascribed to the diabatic paths $4p \to 4d \to 2p \to i$, $4p \to 5d \to 3p$ or $2p \to i$, and $4p \to i$, in the order of increasing energy. A $^3\Pi_g$ contribution is made but is relatively small. For the $4\,^3D$ ionization cross section shown in Fig. 11, in addition to the $^3\Pi_u$ low-energy contribution which also occurs for $3\,^3D$ there is a $^3\Sigma_g^+$ contribution made possible by the asymptotic closeness

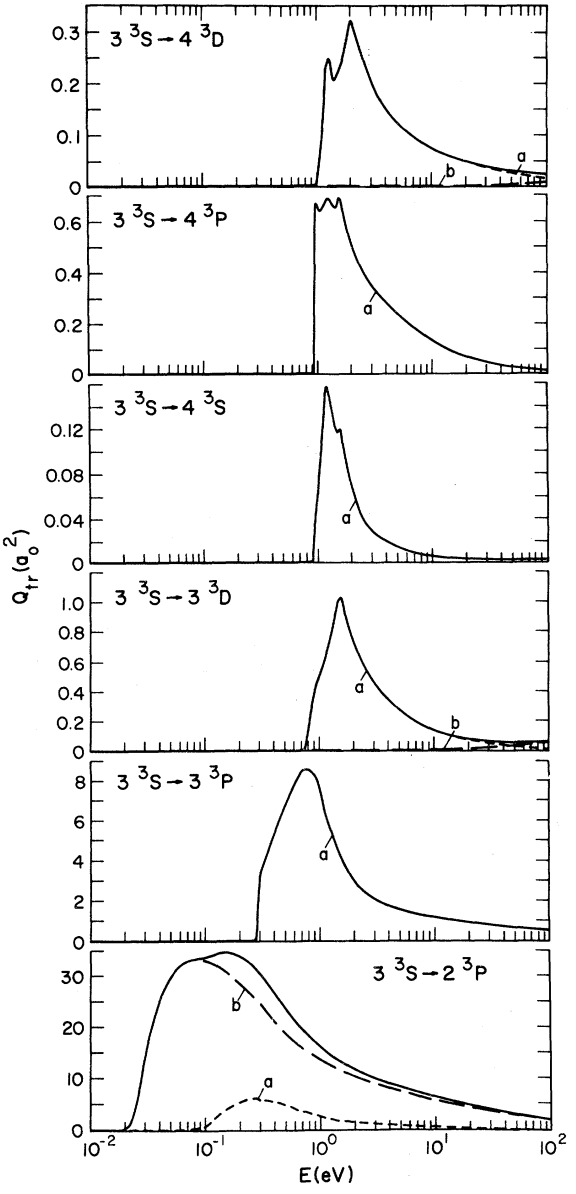

FIG. 12. Excitation-transfer cross sections for He($3\,^3S$) + He($1\,^1S$) collisions. See Fig. 6 for the notation of cross-section components.

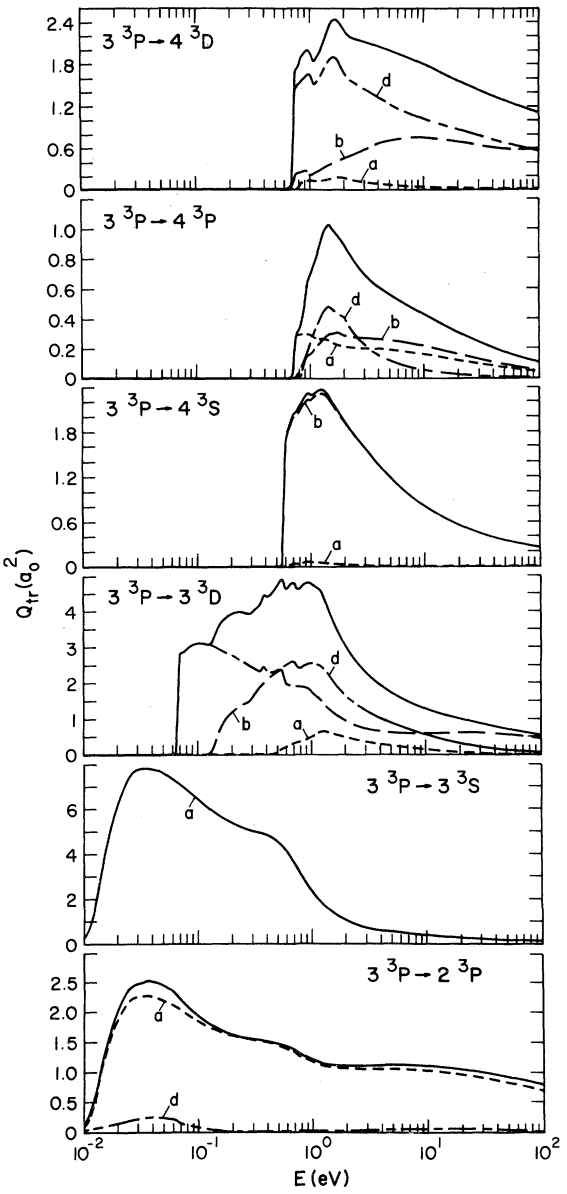

FIG. 13. Excitation-transfer cross sections for He($3\,^3P$) + He($1\,^1S$) collisions. See Fig. 6 for notation.

of the $4d$ and $4f$ levels.

Excitation-transfer cross sections are shown in Figs. 12–14 for collisions of the ground-state atom with the $3\,^3S$, $3\,^3P$, and $3\,^3D$ excited atoms, respectively. These states plus the $2\,^3P$, $4\,^3S$, $4\,^3P$, and $4\,^3D$ are considered as final states. Cross sections for transfer to the $2\,^3S$ from the $n=3$ levels are primarily due to nonadiabatic coupling well away from the curve crossings and are several orders of magnitude smaller than those for transfer to $2\,^3P$ at collision energies of a few eV or less[16]—the cross sections shown for transfer to $2\,^3P$ were actually calculated as the cross sections for transfer to either $2\,^3P$ or $2\,^3S$. The transfer-cross-section components are designated in the same way as they were for the ionization cross sections. In Fig. 12, for $3\,^3S$ collisions, all of the reactions are endothermic except the one yielding the $2\,^3P$ atom, but it too has a nonzero threshold owing to the barrier in the ${}^3\Sigma_u^+$ potential curve. Note that the $3\,^3S \rightarrow 2\,^3P$ cross section is primarily due to ${}^3\Sigma_u^+$ scattering, which makes a negligible contribution in the other cases. For most of the other collisions in Figs. 13 and 14 several symmetries contribute significantly to the transfer cross section. As expected, in most, though not all, cases the primary contribution to exothermic energy transfers comes from the attractive initial curves and the primary contribution to endothermic energy transfers comes from the repulsive initial curves. Excitation-transfer cross sections for transitions between the $n=4$ levels are not presented since long-range couplings between states with the same n, $n \geq 4$, are expected to be important.

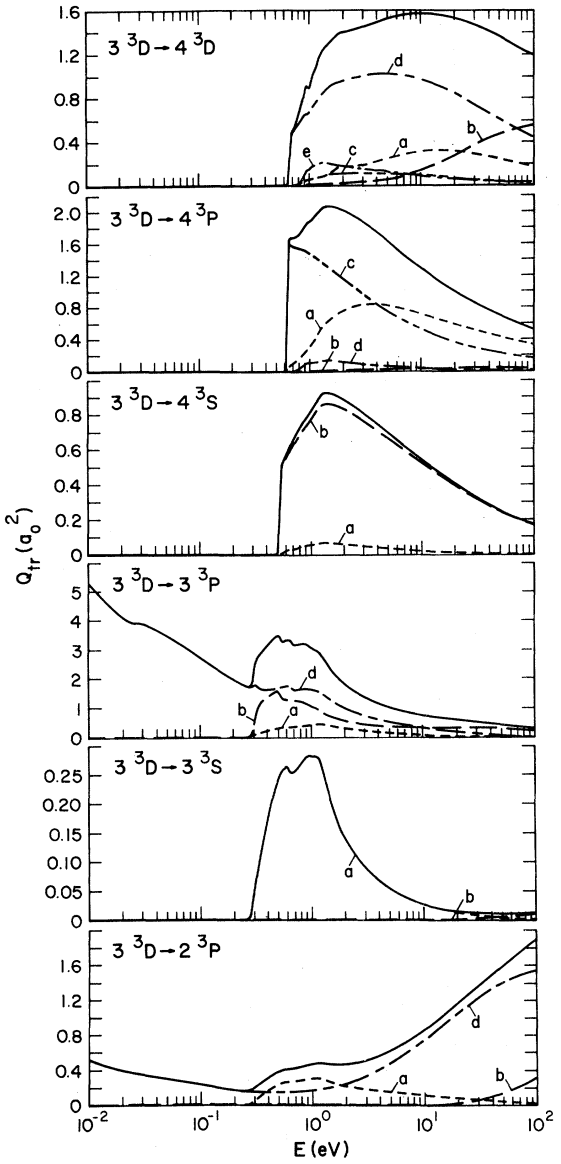

FIG. 14. Excitation-transfer cross sections for $He(3\,^3D) + He(1\,^1S)$ collisions. See Fig. 6 for notation.

The thermally averaged cross sections for $100 \leq T \leq 1000$ °K, assuming a Maxwellian distribution, are given in Table I. Comparison with the available experimental measurements is made in Table II. The measurements of Wellenstein and Robertson,[23,34] who used optical pumping to selectively modulate the various atomic-state populations, are considered to give the most reliable cross sections to date for the $n=3$ reactions. The cross sections at the energy kT are also given in Table II to demonstrate the importance in some cases of the distributional function assumed; in particular the high-energy tail is important for the cross sections which have nonzero thresholds. Considering the simplicity of the model, the agreement with experiment is quite satisfactory. The differences are small enough that they could easily be accounted for by small adjustments of the potential curves and coupling matrix elements.

V. DISCUSSION

Associative ionization and some excitation-transfer processes in helium have been interpreted in terms of a quantitative diabatic-states representation. Instead of doing elaborate quantum-mechanical calculations based on an expansion in this representation, a highly intuitive model was derived to treat the multistate curve-crossing problem which often arises in diabatic representations of scattering processes. The model allows transitions only at curve crossings and assumes that ionization is caused only by electronic coupling in the continuum. The electronic coupling

TABLE I. Thermally averaged theoretical cross sections (in units of 10^{-16} cm^2).[a]

	Temperature (°K)								
	100	200	300	400	600	800	1000	2000	5000
$\bar{Q}_i$ (3^3S)	7×10^{-5}	0.01	0.06	0.14	0.30	0.44	0.53	0.72	0.99
$\bar{Q}_i$ (3^3P)	1.55	2.13	1.99	1.74	1.33	1.08	0.94	0.88	1.37
$\bar{Q}_i$ (3^3D)	4.87	3.57	2.88	2.44	1.93	1.64	1.45	1.06	0.90
$\bar{Q}_i$ (4^3S)	0.20	0.47	0.60	0.65	0.65	0.63	0.61	0.85	2.24
$\bar{Q}_i$ (4^3P)	2.04	1.87	1.66	1.52	1.41	1.42	1.48	1.97	3.07
$\bar{Q}_i$ (4^3D)	5.12	4.56	4.31	4.16	4.02	3.96	3.94	3.95	4.38
$\bar{Q}_{tr}$ ($3^3S\rightarrow2^3P$)	1.16	4.00	5.83	6.92	8.00	8.42	8.53	7.89	5.82
$\bar{Q}_{tr}$ ($3^3S\rightarrow3^3P$)	0	0	2×10^{-4}	2×10^{-3}	0.03	0.10	0.21	0.85	1.47
$\bar{Q}_{tr}$ ($3^3S\rightarrow3^3D$)	0	0	0	0	0	1×10^{-5}	9×10^{-5}	7×10^{-3}	0.08
$\bar{Q}_{tr}$ ($3^3P\rightarrow2^3P$)	0.33	0.52	0.57	0.57	0.55	0.53	0.51	0.45	0.38
$\bar{Q}_{tr}$ ($3^3P\rightarrow3^3S$)	1.01	1.62	1.78	1.81	1.77	1.71	1.65	1.42	0.94
$\bar{Q}_{tr}$ ($3^3P\rightarrow3^3D$)	3×10^{-3}	0.08	0.23	0.37	0.59	0.73	0.83	1.08	1.18
$\bar{Q}_{tr}$ ($3^3D\rightarrow2^3P$)	0.13	0.11	0.09	0.08	0.07	0.07	0.07	0.08	0.11
$\bar{Q}_{tr}$ ($3^3D\rightarrow3^3S$)	0	0	0	5×10^{-5}	7×10^{-4}	3×10^{-3}	6×10^{-3}	0.03	0.05
$\bar{Q}_{tr}$ ($3^3D\rightarrow3^3P$)	1.40	1.16	1.04	0.95	0.84	0.78	0.75	0.76	0.78

[a] Cross sections smaller than 10^{-21} cm^2 are shown as zero.

(configuration interaction)[42] yields much larger ionization cross sections than could be expected from direct vibronic coupling of low-lying adiabatic states to the continuum states[19]; vibronic coupling is expected to be significant only for states lying very near the continuum where there is not an effective purely electronic mechanism for ionization. Angular dynamic coupling between diabatic states was found to be negligible for the transitions considered,[12] with the result that the observable cross sections can be obtained as statistical averages of cross sections for individual molecular symmetries obtained in separate and smaller calculations. The autoionization widths for the diabatic states embedded in the continuum have not yet been calculated but were assumed large. This assumption seems justified for low collision energies where the classical turning points are near the crossing into the continuum. It is expected that the probability per unit time for emitting a near-zero kinetic energy electron, as may occur in the vicinity of the crossing, is large. The observations of Gillen *et al.*[15] that ionization in $He(2\,^3S)+He(1\,^1S)$ collisions occurs with high probability when the continuum is reached and that the electron is generally ejected

TABLE II. Comparison of theoretical and experimental cross sections. Q_{calc} is the calculated cross section at the collision energy $E=kT$; $\bar{Q}_{calc}$ is the thermally averaged cross section at temperature T.

Transition	T (°K)	$\bar{Q}_{exp}$ (10^{-16} cm^2)	$\bar{Q}_{calc}$ (10^{-16} cm^2)	Q_{calc} (10^{-16} cm^2)
$3^3S\rightarrow$ ion	320	<0.01 [a]	0.07	0
$3^3P\rightarrow$ ion	320	1.6 ± 0.1 [a]	1.9	3.2
	400	1.4; 2.1 [b]	1.7	3.5
$3^3D\rightarrow$ ion	320	4.5 ± 0.5 [a]	2.8	3.6
	400	21; 14 [b]	2.4	3.0
	343	146 [c]	2.7	3.4
$3^3P\rightarrow3^3S$	320	2.9 ± 0.3 [d]	1.8	2.2
$3^3D\rightarrow3^3S$	320	<0.01 [d]	6×10^{-6}	0
$3^3P\rightarrow3^3D$	320	0.067 ± 0.005 [d]	0.26	0
$3^3D\rightarrow3^3P$	320	0.62 ± 0.05 [d]	1.02	1.09

[a] Reference 23. Error limits represent random spread of data points and do not include systematic error.

[b] Reference 20.

[c] Reference 21. Measured apparent cross sections for states with $n\geq3$. Since the actual state distribution is not known, no quantitative comparison is possible.

[d] Reference 34. Error limits represent random spread of data points and do not include systematic error.

with very low kinetic energy suggest that this approximation is good at least up to energies on the order of 100 eV. Also, the agreement of the results with experiment seems to provide verification; nevertheless, the approximation should be checked by future calculations.

The derived scattering model includes closed channels, combining them into a single effective potential on an equal footing with the open channels. Tunneling through long-range potential barriers is taken into account by the JWKB approximation. Tunneling into other nonclassical regions could be included in a similar way but is not expected to be very important. Probably the most serious approximation is the neglect of coupling away from the curve crossings. This approximation is quite good for the short-to-intermediate range crossings, and furthermore, the LZ approximation, though not essential to the model, was found to be good for such crossings if one of the states has $n \geq 3$. However, long-range coupling, with or without a curve crossing, is important for some near-resonant transitions between states with the same principal quantum number, $n \geq 4$, and is in fact responsible for the very large cross sections for some of these transitions. Results for such processes have not been presented in the present work, but possibly could be included in the model by approximately separating the long-range and short-range effects. Also, the F and higher angular-momentum states have not been treated since spin-orbit coupling is important in those cases.[36] Another approximation made is the neglect of interference effects arising from multiple trajectories with different phases contributing to the same cross section. This approximation is not considered serious since interference effects are expected to tend to cancel out for a process involving a number of curve crossings, particularly in the integrated cross section. Interference could be included by calculating the complex probability amplitudes rather than the magnitudes as in Sec. II, but the convenience of many of the analytic summations would then be lost. Formulation in terms of a quantum-mechanical optical potential would of course eliminate most of these restrictions but would require orders-of-magnitude more computation. In conclusion, the diabatic-states model has been shown to be a valid and highly physical interpretation of associative ionization in helium and capable of yielding rather accurate cross sections.

---

*Work performed under the auspices of the U. S. Energy Research and Development Administration.

[1]O. Tüxen, Z. Phys. 103, 463 (1936).
[2]F. L. Arnot and M. B. M'Ewen, Proc. R. Soc. A 171, 106 (1939); 166, 543 (1938).
[3]R. Meyerott, Phys. Rev. 70, 671 (1946).
[4]J. A. Hornbeck, Phys. Rev. 84, 615 (1951).
[5]J. A. Hornbeck and J. P. Molnar, Phys. Rev. 84, 621 (1951).
[6]M. S. B. Munson, J. L. Franklin, and F. H. Field, J. Phys. Chem. 67, 1542 (1963); J. S. Dahler, J. L. Franklin, M. S. B. Munson, and F. H. Field, J. Chem. Phys. 36, 3332 (1962).
[7]W. Kaul and R. Taubert, Z. Naturforsch. A 17, 88 (1962); W. Kaul, P. Seyfried, and R. Taubert, Z. Naturforsch. A 18, 432 (1963).
[8]F. J. Comes, Z. Naturforsch. A 17, 1031 (1962).
[9]R. K. Curran, J. Chem. Phys. 38, 2974 (1963).
[10]J. L. Franklin and F. A. Matsen, J. Chem. Phys. 41, 2948 (1964).
[11]B. Liu, Phys. Rev. Lett. 27, 1251 (1971).
[12]J. S. Cohen, preceding paper (referred to as paper I), Phys. Rev. A 13, 86 (1976).
[13]R. S. Mulliken, Phys. Rev. 136, A962 (1964).
[14]J. Stevefelt, Phys. Rev. A 8, 2507 (1973).
[15]K. T. Gillen, D. C. Lorents, R. E. Olson, and J. R. Peterson, J. Phys. B 7, L327 (1974); K. T. Gillen (private communication).
[16]S. A. Evans, J. S. Cohen, and N. F. Lane, Phys. Rev. A 4, 2235 (1971).
[17]J. C. Tully and R. K. Preston, J. Chem. Phys. 55, 562 (1971).
[18]F. Koike and H. Nakamura, J. Phys. Soc. Jpn. 33, 1426 (1972).
[19]S. E. Nielsen and R. S. Berry, Phys. Rev. A 4, 865 (1971); 1, 383 (1970).
[20]M. P. Teter, F. E. Niles, and W. W. Robertson, J. Chem. Phys. 44, 3018 (1966).
[21]J. J. De Corpo and F. W. Lampe, J. Chem. Phys. 51, 943 (1969).
[22]F. Robben, Phys. Rev. A 5, 1516 (1972).
[23]H. F. Wellenstein and W. W. Robertson, J. Chem. Phys. 56, 1077 (1972); H. F. Wellenstein (private communication).
[24]C. B. Collins, B. W. Johnson, and M. J. Shaw, J. Chem. Phys. 57, 5310 (1972).
[25]T. R. Grossheim, J. J. Leventhal, and H. H. Harris, Phys. Rev. A 7, 1591 (1973).
[26]A. H. Gabriel and D. W. O. Heddle, Proc. R. Soc. A 258, 124 (1960).
[27]R. M. St. John and R. G. Fowler, Phys. Rev. 122, 1813 (1961); C. C. Lin and R. M. St. John, Phys. Rev. 128, 1749 (1962); R. M. St. John and T. W. Nee, J. Opt. Soc. Am. 55, 426 (1965).
[28]W. R. Bennett, Jr., P. J. Kindlmann, and G. N. Mercer, Appl. Opt. Suppl. 2, 34 (1965).
[29]W. R. Pendleton, Jr. and R. H. Hughes, Phys. Rev. 138, A683 (1965); R. B. Kay and R. H. Hughes, Phys. Rev. 154, 61 (1967); R. J. Anderson, R. H. Hughes, and T. G. Norton, Phys. Rev. 181, 198 (1969).

[30]R. L. Abrams and G. J. Wolga, Phys. Rev. Lett. 19, 1411 (1967).
[31]S. E. Frish and Y. E. Ionikh, Opt. Spektrosk. 25, 171 (1968) [Opt. Spectrosc. 25, 91 (1968)].
[32]J. Bakos and J. Szigeti, J. Phys. B 1, 1115 (1968).
[33]J. D. Jobe and R. M. St. John, Phys. Rev. A 5, 295 (1972).
[34]H. F. Wellenstein and W. W. Robertson, J. Chem. Phys. 56, 1072 (1972); 56, 1411 (1972).
[35]W. W. Hunter, Jr. and T. E. Leinhardt, J. Chem. Phys. 58, 941 (1973).
[36]C. C. Lin and R. G. Fowler, Ann. Phys. (N. Y.) 15, 461 (1961).
[37]L. Landau, Phys. Z. Sowjetunion 2, 46 (1932); C. Zener, Proc. R. Soc. A 137, 696 (1932); E. C. G. Stueckelberg, Helv. Phys. Acta 5, 369 (1932).
[38]A. Russek, Phys. Rev. A 4, 1918 (1971).
[39]J. C. Y. Chen, Phys. Rev. 156, 12 (1967).
[40]E. Merzbacher, *Quantum Mechanics* (Wiley, New York, 1970), 2nd ed., p. 126.
[41]J. S. Cohen, Bull. Am. Phys. Soc. 20, 252 (1975); 19, 1231 (1974).
[42]U. Fano, Phys. Rev. 124, 1866 (1961).